Journal of Sound and Vibration (1999) **226**(4), 645–674
Article No. jsvi.1999.2316, available online at http://www.idealibrary.com on IDEAL®

CORRELATIONS BETWEEN DYNAMIC STRESS AND VELOCITY IN RANDOMLY EXCITED BEAMS

D. G. KARCZUB AND M. P. NORTON

Department of Mechanical and Materials Engineering, Centre for Acoustics, Dynamics and Vibration, The University of Western Australia, Nedlands, WA 6907, *Australia*

(*Received* 5 *February* 1998, *and in final form* 31 *March* 1999)

Formalized relationships are developed for the estimation of maximum dynamic stress and strain in randomly vibrating structures from simple vibrational velocity measurements obtained using accelerometers. These relationships are based on farfield relationships, factors for the effects of evanescent waves, and the correlation of dynamic stress and velocity spatial maxima in narrow frequency bands. The relationships developed also serve to extend earlier work in this area by providing a consistent theoretical and experimental approach for both narrow band and broad-band resonant vibration, and both resonant and non-resonant vibration. The relationships developed can be applied to the estimation of maximum dynamic stress in the low-, mid- and high-frequency ranges. Theoretical and experimental data are presented demonstrating the basis of these relationships and their application to the measurement of dynamic strain.

1. INTRODUCTION AND LITERATURE REVIEW

Practical procedures using vibrational velocity measurements for the estimation of maximum dynamic stress levels in randomly vibrating structures and piping systems, which are subject to high levels of acoustic, flow-induced or mechanical excitation, are of interest to assess fatigue life and identify potential fatigue failures before they occur. Limitations with the use of strain gauges to measure maximum dynamic stress levels are that (i) the location of maximum dynamic stress for installation of strain gauges is generally not known *a priori*; and (ii) at higher frequencies and short wavelengths, the magnitude of dynamic stress decreases rapidly with distance from boundaries and discontinuities where dynamic stress is usually largest, making the measurement of maximum dynamic stress using finite length strain gauges very difficult. Benefits of using vibrational velocity measurements for the estimation of maximum dynamic stress are that the measurements are easily performed, the transducers are portable and robust, it is not necessary to know the location of maximum dynamic stress, and the positioning of transducers is not critical to the accuracy of dynamic stress predictions.

0022-460X/99/390645 + 30 $30.00/0

Relationships between dynamic stress and velocity were first derived by Hunt [1] and Ungar [2]. One of the main outcomes of their work was that the ratio of dynamic stress to velocity is frequency independent in simple beams and plates vibrating at resonance. Their work included the correlation of dynamic stress and velocity spatial maxima in structures vibrating at resonance, and was subsequently applied by Wachel [3] to the estimation of maximum dynamic stress in piping systems vibrating at their first resonant mode using simple measurements of maximum overall velocity.

The relationships derived by Hunt [1] and Ungar [2] have been extended to the broad-band multi-modal resonant vibration of plates and large diameter cylindrical shells by Stern [4]. The relationships derived by Stearn are based on the correlation of spatial averages of dynamic stress and velocity, and require factors to relate spatial maximum levels of dynamic stress to spatially averaged levels of dynamic stress. The relationships also assume a diffuse wave field which requires that at least 10 modes are excited in the frequency band of interest for the relationships to be valid. The relationships derived by Stearn were developed for Statistical Energy Analysis applications and are adopted for the prediction of dynamic stress in Statistical Energy Analysis applications by Lyon [5].

Experimental investigations of correlations between dynamic stress and velocity are limited to those by Stearn [4] for broad-band vibration of plates and large diameter cylindrical shells, and Norton and Fahy [6] for broad-band vibration of fluid-filled cylindrical shells. Both of these investigations correlate the spatial averages of dynamic stress and velocity using diffuse wave field assumptions. Stearn [4, 7] also investigated the dynamic stress concentration at a step change in thickness of a plate as part of theoretical and experimental investigations to relate spatial maximum levels of dynamic stress with spatially averaged values. Dynamic stress concentration is an increase in dynamic stress at a boundary or a discontinuity due to evanescent wave effects [8, 9]. Norton and Fahy also reported dynamic stress concentration effects in their experiments.

In the present paper, travelling wave solutions are used to derive farfield relationships between the propagating wave components of dynamic stress and velocity. Formal relationships for the correlation of dynamic stress and velocity spatial maxima are then defined. These latter relationships incorporate explicit factors for the effects of evanescent waves on dynamic stress and velocity, and are based on analyses of dynamic stress and velocity spatial distributions. Factors for the effects of evanescent waves are subsequently incorporated in a single overall factor relating the spatial maxima of dynamic stress and velocity. The relationships derived here are for the flexural vibration of thin beams. Similar relationships have also been derived for the longitudinal and torsional vibration of thin beams, the flexural vibration of thin rectangular plates, and the coupled longitudinal, torsional and flexural vibration of cylindrical shells [9].

The present work serves to extend earlier work in this area by providing a consistent approach with a firm theoretical basis for narrow-band and broad-band vibration, and for resonant and non-resonant vibration. The relationships derived can be applied in the low-, mid- and high-frequency ranges and are independent of the type and amplitude of excitation. This is achieved by

correlating the spatial maxima of dynamic stress and velocity in each frequency band to predict the spatial maximum dynamic stress in each frequency band, and then summing these values to obtain a conservative prediction of maximum overall dynamic stress. The correlation of dynamic stress and velocity spatial maxima directly takes into account dynamic stress concentration effects.

2. TRAVELLING WAVE EQUATIONS

The travelling wave solution to the governing differential equation for flexural vibration of a beam, neglecting shear strain and rotary inertia, is described by two propagating waves moving in opposite directions and two evanescent waves decaying from opposite ends of the beam. In farfield regions, the evanescent waves are not significant to the response and the evanescent wave terms can be neglected. The complete and farfield forms of the travelling wave solution for velocity at a given frequency f are

$$\mathbf{v}(x, f) = \mathrm{i}2\pi f(\mathbf{A}_1 \mathrm{e}^{-\mathrm{i}kx} + \mathbf{A}_2 \mathrm{e}^{\mathrm{i}kx} + \mathbf{A}_3 \mathrm{e}^{-kx} + \mathbf{A}_4 \mathrm{e}^{kx}) \tag{1}$$

and

$$\mathbf{v}_{FF}(x, f) = \mathrm{i}2\pi f(\mathbf{A}_1 \mathrm{e}^{-\mathrm{i}kx} + \mathbf{A}_2 \mathrm{e}^{\mathrm{i}kx}), \tag{2}$$

respectively, where $\mathbf{v}$ is the complex velocity, x is the position along the beam axis, k is the wavenumber (which is complex if damping is included), i is $\sqrt{1}$ and the $\mathbf{A}_j$ are complex constants which vary with frequency. The travelling wave solutions for dynamic bending stress and dynamic bending strain are given by

$$\boldsymbol{\sigma}(x, f) = E\xi(x, f) = Ey_m k^2[(\mathbf{A}_1 \mathrm{e}^{-\mathrm{i}kx} + \mathbf{A}_2 \mathrm{e}^{\mathrm{i}kx}) - (\mathbf{A}_3 \mathrm{e}^{-kx} + \mathbf{A}_4 \mathrm{e}^{kx})] \tag{3}$$

for vibration at any location along the beam, where σ is complex stress, ξ is complex strain, E is the modulus of elasticity and y_m is the distance of the outermost fibre from the centroidal axis, and by

$$\boldsymbol{\sigma}_{FF}(x, f) = E\boldsymbol{\xi}_{FF}(x, f) = Ey_m k^2(\mathbf{A}_1 \mathrm{e}^{-\mathrm{i}kx} + \mathbf{A}_2 \mathrm{e}^{\mathrm{i}kx}) \tag{4}$$

in the farfield. The constants $\mathbf{A}_1$–$\mathbf{A}_4$ are the same for equations (1)–(4) and are calculated using the travelling wave modelling procedures described in Karczub [9].

3. FARFIELD RELATIONSHIPS

The dynamic bending stress for flexural vibration of a beam is related to the transverse velocity at the same location by a frequency-independent constant if the evanescent wave components are neglected. Dividing the farfield dynamic stress in equation (4) by the farfield velocity in equation (2) yields

$$\frac{\boldsymbol{\sigma}_{FF}(x, f)}{\mathbf{v}_{FF}(x, f)} = \frac{Ey_m k^2}{\mathrm{i}2\pi f} = -\mathrm{i}Ey_m \sqrt{\frac{\rho A}{EI}} = -\mathrm{i}E\frac{K_{shape}}{c_L}, \tag{5}$$

where $K_{shape} = y_m\sqrt{A/I}$ is a non-dimensional geometric shape factor, $c_L = \sqrt{E/\rho}$ is the longitudinal wave speed, ρ is density, A is cross-sectional area, and I is the area moment of inertia. The relationship in equation (5) states that the complex farfield dynamic stress at position x is related to the complex farfield velocity at the same position by a phase shift of $-\mathrm{i}$ and the frequency independent constant EK_{shape}/c_L. The frequency-independent constant is a function of only cross-sectional geometry, density and the modulus of elasticity. The relationship in equation (5) is based on the dynamic response due to propagating waves alone in the absence of evanescent waves, but is also applicable in farfield response regions where the contribution of evanescent waves to the response is negligible.

The non-dimensional geometric shape factor K_{shape} in equation (5) is simple to calculate and lies in a small range for different cross-sections. The value of the geometric shape factor for both solid rectangular bars and solid circular bars is independent of cross-sectional dimensions. It is equal to $\sqrt{3}$ for a solid rectangular bar and to 2 for a solid circular bar [1]. For a hollow bar or cylinder, the geometric shape factor is a function of the diameter ratio d_i/d_o being given by $K_{shape} = 2\sqrt{1(1 + (d_i/d_o)^2)}$, where d_i is the inside diameter and d_o is the outside diameter. The geometric shape factor for a hollow bar lies in the range of $\sqrt{2}$ for a very thin-walled cylinder, to 2 for a solid circular bar.

3.1. FARFIELD RELATIONSHIPS FOR THE PREDICTION OF DYNAMIC STRESS

The relationship in equation (5) finds use in the two-accelerometer method for structural intensity measurements and can also be used to determine dynamic stress or dynamic strain from velocity in farfield regions. The prediction of dynamic stress or dynamic strain from velocity may be in the form of either spectral or time history predictions. Theoretical relationships for the prediction of dynamic stress and dynamic strain from velocity in farfield regions are presented in the following paragraphs.

3.1.1. *Frequency–domain predictions*

Re-arranging equation (5), the complex dynamic bending stress at any farfield position can be predicted directly from the complex velocity at the same position by scaling the complex velocity by the factor $-\mathrm{i}EK_{shape}/c_L$; hence,

$$\boldsymbol{\sigma}_{FF}(x, f) = E\boldsymbol{\xi}_{FF}(x, f) = -\mathrm{i}E\frac{K_{shape}}{c_L}v_{FF}(x, f) \tag{6}$$

In terms of mean-square values, the dynamic stress is related to velocity by

$$\langle\sigma^2_{FF}(x, f)\rangle = \left(E\frac{K_{shape}}{c_L}\right)^2\langle v^2_{FF}(x, f)\rangle \tag{7}$$

and the dynamic strain is related to velocity by

$$\langle\xi^2_{FF}(x, f)\rangle = \left(\frac{K_{shape}}{c_L}\right)^2\langle v^2_{FF}(x, f)\rangle. \tag{8}$$

Therefore, auto-spectral measurements of velocity in the farfield can be used to predict auto-spectra of either dynamic stress or dynamic strain at the same location as the velocity measurement. Similar narrow-band relationships are given by Hunt [1] and Ungar [2] based on mode shapes for vibration at a single natural frequency. By repeating the velocity measurements at a number of locations, these relationships can be used to determine farfield spatial distributions of dynamic stress (or dynamic strain) in each frequency band. The factor EK_{shape}/c_L in equation (7), which relates dynamic stress to vibrational velocity, is defined here as the farfield correlation ratio for dynamic stress; similarly, the factor K_{shape}/c_L in equation (8) is defined as the farfield correlation ratio for dynamic strain.

3.1.2. *Overall mean-square predictions*

Since the farfield relationship between dynamic stress and velocity for flexural vibration of a beam is frequency independent, it can also be used to relate overall mean-square value of dynamic stress and velocity. Summing the mean-square response in equation (7) over each frequency f gives

$$\langle \sigma_{FF}^2(x) \rangle = \left(E \frac{K_{shape}}{c_L} \right)^2 \langle v_{FF}^2(x) \rangle \tag{9}$$

and similarly for dynamic strain using equation (8).

3.1.3. *Time–domains predictions*

The relationships in equation (6) are also applicable to time history predictions of dynamic stress and dynamic strain from velocity. Dynamic stress and dynamic strain time histories are predicted from a velocity time history by introducing a phase shift of $-\mathrm{i}$ into the velocity time history and scaling the time history by the farfield correlation ratio. This may be stated mathematically as

$$\xi(t) = \frac{EK_{shape}}{c_L} \int_{-\infty}^{\infty} -\mathrm{i} \left\{ \int_{-\infty}^{\infty} v(t) \mathrm{e}^{-\mathrm{i}2\pi f t} \, \mathrm{d}t \right\} \mathrm{e}^{\mathrm{i}2\pi f t} \, \mathrm{d}f. \tag{10}$$

In practise the phase shift of $-\mathrm{i}$ can be implemented digitally using a combination of Fourier transform methods, frequency-domain processing and convolution. This procedure may find use for cycle counting fatigue predictions at farfield locations.

3.2. GENERALIZATION OF FARFIELD RELATIONSHIPS FOR THE PREDICTION OF MAXIMUM DYNAMIC STRESS

In general, the dynamic stresses and dynamic strains in a beam due to flexural vibration can be predicted in farfield regions from velocity using only the farfield correlation ratio and a phase shift of $-\mathrm{i}$. For mean-square predictions, the phase shift of $-\mathrm{i}$ can be neglected and only the farfield correlation ratio is required. Since the above relationships between dynamic bending stress and velocity in the farfield are also independent of structural details such as beam length and boundary

conditions, it would be useful if the same relationships could also be applied in nearfield regions. Spatial distributions presented in the next section show that dynamic stress is not simply related to the velocity at the same location in nearfield regions, but that the spatial maxima of dynamic stress and velocity at each frequency may be correlated using the same generic relationship as in equation (7). This is achieved by incorporating an additional factor in equation (7) for the effects of evanescent waves on the propagating wave component of the dynamic response. The correlation of dynamic stress and velocity spatial maxima is considered in section 5.

4. DYNAMIC STRESS AND VELOCITY NARROW-BAND SPATIAL DISTRIBUTIONS

Narrow-band spatial distributions of dynamic stress and velocity are presented in the following sub-sections for the flexural vibration of some point-excited beam systems. These spatial distributions demonstrate nearfield effects, dynamic stress concentration, and correlations between dynamic stress and velocity. The beam system dimensions are taken from the beams tested experimentally in section 6 [9], so that the theoretical calculations presented here are comparable with the experimental results. The structural damping coefficient used in all calculations is 0·04 unless specified otherwise. This is the level of damping estimated for the clamped beam experimental rig [9].

4.1. CLAMPED BEAM SYSTEM

Spatial distributions of dynamic stress, farfield dynamic stress and nearfield dynamic stress are plotted in Figure 2 for the first three natural frequencies of the clamped beam system in Figure 1. The farfield dynamic stress represents the propagating wave component of dynamic stress and the nearfield dynamic stress represents the evanescent wave component of dynamic stress.

The velocity, farfield velocity and nearfield velocity response components are also plotted in Figure 2 but in the form of dynamic stress predictions obtained by scaling the velocity response components by the farfield correlation ratio. Since these velocity components are related to their respective dynamic stress

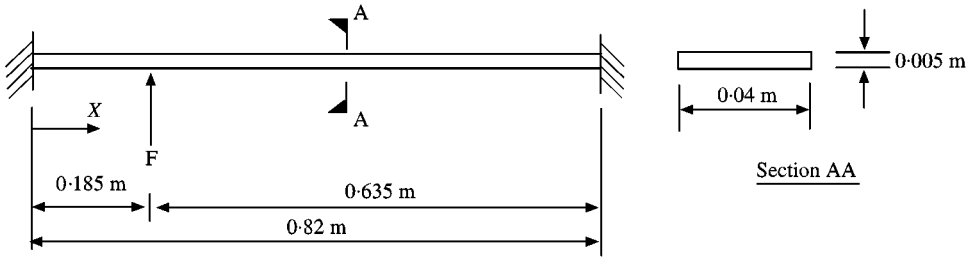

Figure 1. Thin beam clamped at both ends and excited by a unit point force at $x = 0{\cdot}185$ m.

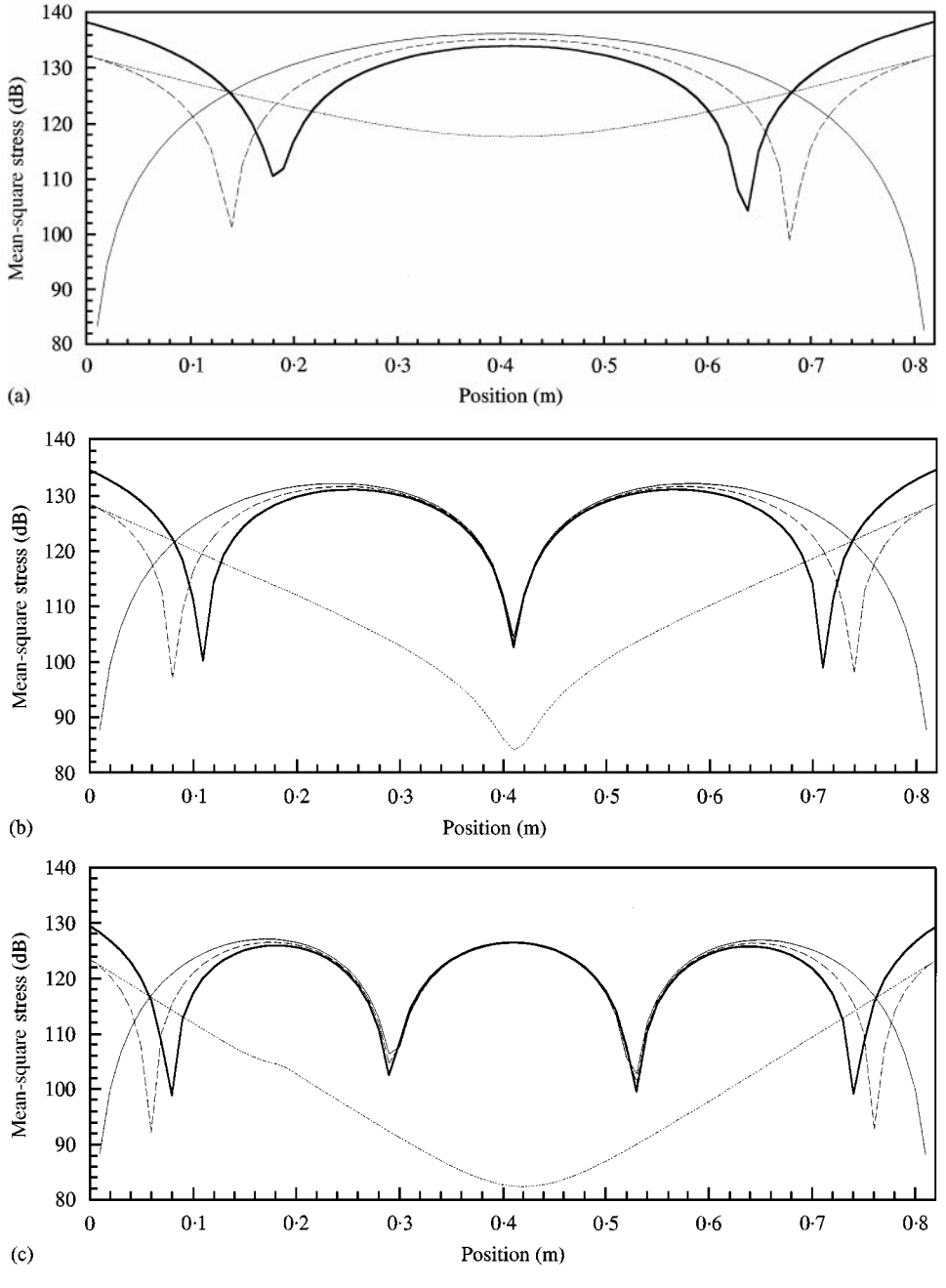

Figure 2. Calculated spatial distributions of dynamic stress and predicted dynamic stress in a clamped beam (dB re 1 N/m^2) (—— stress; —— predicted stress from velocity; – – – farfield stress; - - - nearfield stress). (a) 1st Natural Frequency (38·5 Hz). (b) 2nd Natural Frequency (106 Hz). (c) 3rd Natural Frequency (208 Hz).

components by the farfield correlation ratio, the farfield velocity is represented by the farfield dynamic stress curve and the nearfield velocity is represented by the nearfield dynamic stress curve.

4.1.1. *Nearfield and farfield regions*

The clamped beam in Figure 1 has boundary conditions that result in flexural nearfields adjacent to each of the clamped boundaries. The nearfields are identified by regions in which the response is different to the propagating wave component of the response due to the presence of significant evanescent waves. At low frequencies the clamped boundary nearfields span most or all of the beam. This is seen in Figures 2(a) and 2(b) for vibration at the first two natural frequencies. As frequency is increased and wavelengths decrease, the spatial extent of each nearfield decreases, and a farfield region forms at the centre of the beam which has increasing spatial extent with frequency. The spatial distributions in Figure 2(c), for vibration at the third natural frequency, are representative of the vibrational response fields at higher frequencies where both nearfield and farfield regions exist.

At non-resonant frequencies there are additional evanescent waves that emanate from the excitation position. These evanescent waves are due to a force discontinuity at the position where the exciting force is applied. This is demonstrated in Figure 3 for vibration at a non-resonant frequency between the second and third natural frequencies. The evanescent waves that emanate from the force discontinuity are not observed for vibration at the various natural frequencies considered in Figure 2 since the impedance associated with a point force applied to a lightly damped beam is small or negligible at resonance; and in an undamped structure vibrating at resonance there are no evanescent waves generated by a force discontinuity such as this. It should be noted that a normal modes summation model for the forced vibration of a point excited beam (based on the undamped modes for free vibration) gives erroneous results in the region where the point force is applied and should not be used for the analysis of dynamic stress at non-resonant frequencies. Increasing the number of terms in the modal summation will not overcome this problem since the normal modes used in the summation do not include the evanescent waves that emanate from the point of excitation at non-resonant frequencies.

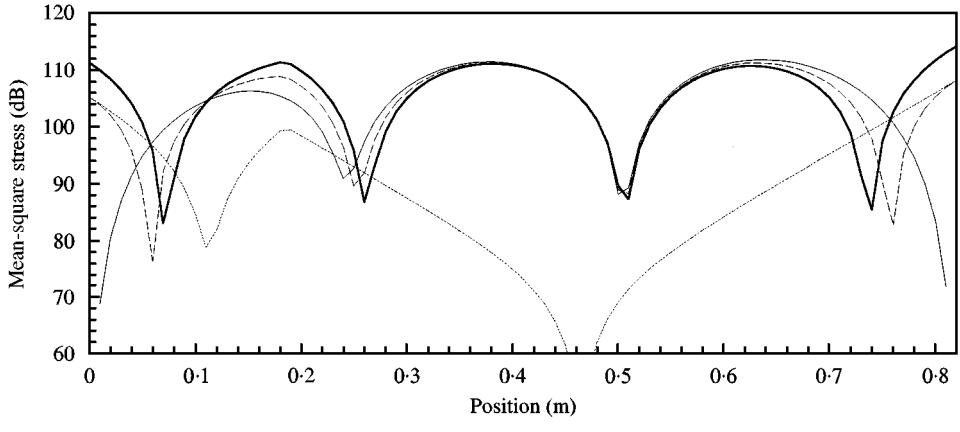

Figure 3. Calculated spatial distributions of dynamic stress and predicted dynamic stress in a point excited clamped beam for vibration at the non-resonant frequency, $f = 180$ Hz (dB re 1 N/m^2) (——stress; —— predicted stress; – – – farfield stress; - - - nearfield stress).

4.1.2. *Effects of evanescent waves*

The general effects of evanescent waves on the propagating wave components of the beam response are to increase one of dynamic stress and velocity, and to decrease the other. At the clamped boundaries in Figure 2 for instance, dynamic stress is increased compared with farfield dynamic stress, and velocity is decreased compared with farfield velocity levels; whilst further from the clamped boundaries the dynamic stress is decreased and the velocity is increased. Similar effects are observed in the excitation region for vibration at non-resonant frequencies (Figure 3). The opposite effects of evanescent waves on the propagating wave components of dynamic stress and velocity are due to the opposite phase of evanescent waves in the dynamic stress and velocity travelling wave solutions, given by equations (3) and (1) respectively.

4.1.3. *Predictions of dynamic stress based on farfield relationships*

Due to the opposite effects of evanescent waves on the dynamic stress and velocity response, velocity predictions of dynamic stress based on the farfield relationships derived in Section 3 are only accurate in farfield regions. As maximum dynamic stress may occur in the nearfield, as was the case for the beam system considered in this sub-section, farfield relationships between dynamic stress and velocity at the same position are inadequate for the prediction of maximum dynamic stress in a structure. Maximum dynamic stress levels are required for calculations of fatigue life.

4.1.4. *Dynamic stress concentration*

The increase in maximum dynamic stress at the clamped boundary (and at the excitation position for non-resonant frequencies) above maximum farfield dynamic stress levels due to evanescent waves is referred to as dynamic stress concentration [8]. Dynamic stress concentration is therefore the result of flexural nearfields and leads to maximum dynamic stress at nearfield locations. Evanescent waves also increase the spatial maximum of velocity above the spatial maximum farfield velocity, although the increase in maximum velocity is less than the increase in maximum dynamic stress for this system.

4.1.5. *Locations of maximum response*

Due to the opposite effects of evanescent waves on the dynamic stress and velocity response, the positions of maximum dynamic stress and maximum velocity occur at different locations. For resonant vibration of the clamped beam, the position of maximum dynamic stress is always at a clamped boundary, whereas maximum velocity occurs at a different location at each frequency.

4.1.6. *Implications for strain gauge measurements*

Dynamic stress decreases rapidly in magnitude with distance from the clamped boundaries due to the presence of significant evanescent waves, particularly at

higher frequencies as wavelengths decrease. To accurately measure the maximum dynamic stress at clamped boundaries, the strain gauges must be sufficiently short and located as close as possible to the boundaries. This has significant implications for cycle counting predictions of fatigue in broad-band excited systems since the dynamic strain is difficult to measure right at the boundary of the system. As cycle counting fatigue predictions are sensitive to the exact time history used, the use of dynamic strain data from an offset measurement position may yield inaccurate results.

4.2. SIMPLY SUPPORTED BEAM WITH A CONCENTRATED MASS

Spatial distributions of dynamic stress and velocity are presented in this sub-section for the flexural vibration of a simply supported beam with a concentrated mass at its midspan. Fatigue failures commonly occur in systems with large concentrated masses [3]. The system with a concentrated mass analyzed here is shown schematically in Figure 4.

4.2.1. *Spatial distributions*

The spatial distributions of dynamic stress and velocity for vibration at the first, third and ninth natural frequencies of the simply supported beam with the concentrated mass are plotted in Figure 5. There are no evanescent waves associated with the pinned boundaries of this system, but there are significant evanescent waves decaying from either side of the concentrated mass. These evanescent waves are present in the system to satisfy a force discontinuity at the centre of the beam which is due to the inertia of the concentrated mass.

4.2.2. *Evanescent wave effects at the lowest natural frequency*

At the first natural frequency of the system in Figure 4, the evanescent waves associated with the concentrated mass are significant over the whole beam. Their effect is to increase dynamic stress compared with the farfield dynamic stress at all locations along the beam, and to decrease velocity compared with the farfield velocity at all locations along the beam. This is an unusual case since the maximum velocity is significanatly less than the maximum farfield velocity, whereas in other systems considered [9] the maximum velocity is increased above the maximum farfield velocity in the presence of evanescent waves. The increase in maximum dynamic stress above the maximum farfield dynamic stress is the same as for other systems.

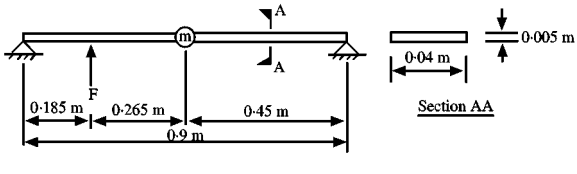

Figure 4. Simply supported beam with a concentrated mass excited by a unit point force.

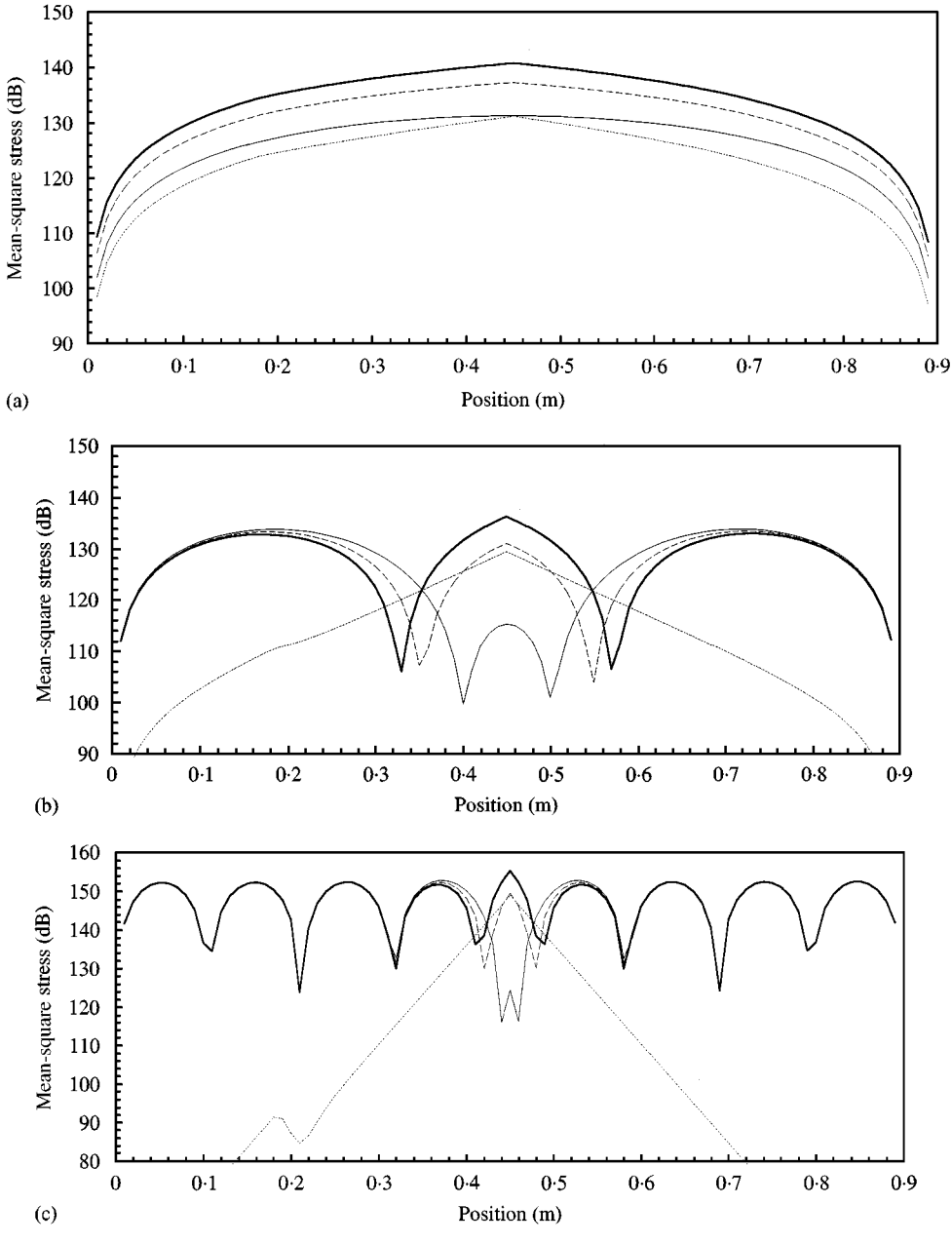

Figure 5. Calculated spatial distributions of dynamic stress and predicted dynamic stress in a simply supported beam with a concentrated mass at $x = 0{\cdot}45$ m (dB re 1 N/m^2) (—— stress; —— predicted stress; – – – farfield stress; - - - nearfield stress). (a) 1st Natural Frequency (5·5 Hz). (b) 2nd Natural Frequency (92·5 Hz). (c) 9th Natural Frequency (1022 Hz).

4.2.3. *Evanescent wave effects at higher natural frequencies*

Evanescent waves for vibration at the odd natural frequencies above the first natural frequency of this system have a different effect than at the first natural

frequency and produce nearfield effects similar to those observed in the previous sub-section. In the region nearest the concentrated mass, dynamic stress levels are increased above the propagating wave component of the response and velocity is decreased below the propagating wave component of the response. Further from the concentrated mass, dynamic stress is decreased and velocity is increased in comparison with propagating wave component of the response. Outside the nearfield region, both dynamic stress and velocity are equal to their respective propagating wave components and dynamic stress can be predicted from velocity using the farfield correlation ratio. Spatial distributions to either side of the concentrated mass are very similar to the spatial distributions in the region of a clamped boundary (see section 4.1).

5. CORRELATION OF DYNAMIC STRESS AND VELOCITY SPATIAL MAXIMA

The spatial distributions presented in section 4 show that simple farfield relationship between dynamic stress and velocity at the same point can be used to predict dynamic stress from velocity in farfield regions, but that the same relationships do not apply at a point in the nearfield. This is due to the opposite effects of evanescent waves on the propagating wave components of dynamic stress and velocity in nearfield regions. It was also observed that maximum dynamic stress usually occurs in the nearfield due to dynamic stress concentration associated with evanescent waves.

The farfield relationships between dynamic stress and velocity that were derived in section 3 can be extended to the prediction of maximum dynamic stress from velocity. This is achieved by using equation (7) to relate the spatial maxima of the propagating wave components of dynamic stress and velocity, and introducing factors for the effects of evanescent waves on the spatial maxima of dynamic stress and velocity. Thus, equation (7) is used to obtain a generalized relationship between the spatial maxima of dynamic stress and velocity.

5.1. FACTORS FOR THE EFFECTS OF EVANESCENT WAVES

The general effects of evanescent waves are to increase maximum dynamic stress and maximum velocity above maximum farfield levels, but by different amounts and at different locations. If $\sigma_{max}(f)/\sigma_{max,FF}(f)$ is the increase in maximum dynamic stress above the maximum farfield dynamic stress and $v_{max}(f)/v_{max,FF}(f)$ is the increase in maximum velocity above the maximum farfield velocity, then the ratio of maximum dynamic stress to maximum velocity is given by

$$\frac{\sigma_{max}(f)}{v_{max}(f)} = \frac{\sigma_{max}(f)/\sigma_{max,FF}(f)}{v_{max}(f)/v_{max,FF}(f)} \frac{EK_{shape}}{c_L} \tag{11}$$

If we let

$$K'(f) = \frac{\sigma_{max}(f)/\sigma_{max,FF}(f)}{v_{max}(f)/v_{max,FF}(f)}, \tag{12}$$

then equation (11) becomes

$$\frac{\sigma_{max}(f)}{v_{max}(f)} = \frac{E\xi_{max}(f)}{v_{max}(f)} = K'(f)\frac{EK_{shape}}{c_L} \tag{13}$$

The factor $K'(f)$ represents the increase or decrease in the farfield correlation ratio due to the effects of evanescent waves on the dynamic response. This factor also represents the relative increase in maximum dynamic stress levels above maximum farfield levels compared with the increase in maximum velocity above maximum farfield levels.

5.2. GENERALIZED RELATIONSHIPS

The relationship in equation (13) states that the maximum dynamic stress in a structure is related to the maximum velocity by the farfield correlation ratio and a frequency-dependent factor, $K'(f)$. Defining

$$K(f) = K'(f)K_{shape}, \tag{14}$$

the ratio of maximum dynamic stress to maximum velocity is re-expressed as

$$\frac{\sigma_{max}(f)}{v_{max}(f)} = \frac{E\xi_{max}(f)}{v_{max}(f)} = E\frac{K(f)}{c_L} \tag{15}$$

where $K(f)$ is defined as the non-dimensional correlation ratio between dynamic strain and velocity, $EK(f)/c_L$ is defined as the correlation ratio for dynamic stress, and $K(f)/c_L$ is defined as the correlation ratio for dynamic strain.

5.3. RELATIONSHIPS FOR THE PREDICTION OF MAXIMUM DYNAMIC STRESS

Practical relationships for autospectral, overall and time-domain predictions of maximum dynamic stress are summarized in the following paragraphs.

5.3.1. *Mean-square dynamic stress*

The spatial maximum of mean-square dynamic stress is predicted from the spatial maximum mean-square velocity using the relationship

$$\langle\sigma^2_{max}(f)\rangle = \left(E\frac{K(f)}{c_L}\right)^2 \langle v^2_{max}(f)\rangle. \tag{16}$$

and spatial maximum mean-square dynamic strain is given by

$$\langle\xi^2_{max}(f)\rangle = \left(\frac{K(f)}{c_L}\right)^2 \langle v^2_{max}(f)\rangle. \tag{17}$$

These relationships are derived directly from equation (15) for vibration at frequency f. It should be noted that unlike equation (5) in section 2.2.2, these relationships between dynamic stress and velocity are not directly applicable to the time-domain analysis of dynamic stress.

5.3.2. *Overall mean-square dynamic stress*

A conservative prediction of the maximum overall mean-square dynamic stress is obtained by constructing a spectrum of maximum predicted mean-square dynamic stress in each frequency band f_i from equation (16), and then summing the mean-square values in each frequency band:

$$\langle \sigma^2_{max} \rangle \leqslant \sum_{i=1}^{\infty} \langle \sigma^2_{max}(f_i) \rangle. \tag{18}$$

Equation (18) is exact is cases where the maximum dynamic stress in each frequency band occurs at the same location for all frequencies f_i. An example of a system with maximum dynamic stress at the same location at virtually all frequencies is the clamped beam system in section 4.1. For systems that do not have maximum dynamic stress at the same location at all frequencies, this approach provides a conservative upper-bound prediction of the maximum overall mean-square dynamic stress.

5.3.3. *Peak dynamic stress in the time-domain*

The frequency-domain approach for predicting the maximum overall mean-square dynamic stress which is based on narrow-band correlations between dynamic stress and velocity cannot be used for time-history predictions of dynamic strain. It may, however, be used to estimate peak dynamic stress in the time-domain at the location of maximum overall dynamic stress. This involves the use of a crest factor to relate the peak and root-mean-square levels of dynamic stress. The crest factor is defined by

$$Crest\ Factor = \frac{Peak\ \ Level}{Root\text{-}Mean\text{-}Square\ \ Level}. \tag{19}$$

Applying the definition of the crest factor in equation (19), the maximum peak dynamic stress is calculated directly from the maximum overall mean-square dynamic stress:

$$[\sigma(t)]_{max} = Crest\ Factor \times \langle \sigma^2_{max} \rangle^{1/2}. \tag{20}$$

The crest factor in equation (20) can be determined for the system being analyzed by measuring the peak and root-mean-square velocities at a selected location, and then calculating the crest factor according to equation (19).

5.4. CORRELATION RATIO CALCULATION PROCEDURES

Procedures for determining correlation ratios are outlined below.

5.4.1. *Non-dimensional correlation ratio*

The non-dimensional correlation ratio factor $K(f)$ in equation (15) is calculated using either numerically or experimentally determined ratios of maximum dynamic

stress to maximum velocity. If the spatial maxima of dynamic stress and velocity are known for a given structure, then $K(f)$ is readily calculated from the definition of the correlation ratio in equation (15):

$$K(f) = \frac{c_L}{E}\frac{\sigma_{max}(f)}{v_{max}(f)} = c_L\frac{\xi_{max}(f)}{v_{max}(f)}. \tag{21}$$

Similarly, if $\sigma_{max,\,pred} = Ev_{max}/c_L$ is the maximum predicted dynamic stress based upon the farfield correlation ratio, the non-dimensional correlation ratio $K(f)$ is calculated from

$$K(f) = \frac{\sigma_{max}(f)}{\sigma_{max,\,pred}(f)} = \frac{\xi_{max}(f)}{\xi_{max,\,pred}(f)}. \tag{22}$$

The correlation ratio is then calculated directly from $K(f)$ using the definition for the correlation ratio given in section 5.2.

5.4.2. *Correlation ratios for resonant vibration*

The correlation ratio for mode n at the natural frequency f_n is given by

$$\frac{EK(f_n)}{c_L} = \frac{\sigma_{max,n}}{v_{max,n}}, \tag{23}$$

where $\sigma_{max,n}$ is the maximum dynamic stress of mode n and $v_{max,mn}$ is the maximum velocity of mode n. Since the ratio of maximum dynamic stress to maximum velocity in equation (23) is independent of the response amplitude, the spatial maxima of dynamic stress and velocity obtained from a normal mode calculation can be used to evaluate the correlation ratio. (In a normal mode calculation, $\sigma_{max,n}$ and $v_{max,n}$ are for an arbitrary amplitude of vibration determined by a user-selected normalization of the displacement vector.) Normal mode calculations are readily implemented using a finite element package with dynamic analysis capabilities.

To perform these calculations only the structural details of the system being analyzed are required. It is not necessary to know the type of excitation, its spatial distribution, the amplitude of excitation, or the damping in the structure. The availability of normal mode calculations for determining the correlation ratio is very useful since the excitation and damping are usually not known or are difficult to describe. Resonant calculations of the correlation ratio will usually be sufficient since most systems for which dynamic stress is of interest are resonant.

5.4.3. *Correlation ratios for non-resonant vibration*

The farfield relationship between the propagating wave components of dynamic stress and velocity represents the underlying principle in the correlation of dynamic stress and velocity spatial maxima. Since this relationship is independent of whether the response is resonant or non-resonant, the correlation ratio should be

similar at resonant and non-resonant frequencies. Hence there exists the possibility of using resonant values of the correlation ratio at non-resonant frequencies. This is exemplified by calculations of the non-dimensional correlation ratio $K(f)$ presented in the next section. Based on these results we may assume that the readily determined correlation ratios for resonant vibration can be applied at non-resonant frequencies to obtain predictions of maximum overall dynamic stress in narrow-band and broad-band excited systems vibrating above their first natural frequency. This involves using the larger of the resonant correlation ratios for the natural frequencies bounding the frequency of interest as the correlation ratio for vibration at that frequency.

5.5. BROAD-BAND CALCULATIONS OF THE NON-DIMENSIONAL CORRELATION RATIO

The non-dimensional correlation ratio $K(f)$ is plotted over a range of frequencies in this section to demonstrate the boundedness of $K(f)$ for resonant and non-resonant frequencies, to assess the effects of a concentrated mass on $K(f)$, and to show that correlations between dynamic stress and velocity are not applicable below the first natural frequency.

5.5.1. *Clamped beam*

The non-dimensional correlation ratio $K(f)$ is plotted in Figure 6 for vibration of the point-excited clamped beam in Figure 1 at a range of frequencies starting below the first natural frequency. $K(f)$ is equal to 2·3 at the first natural frequency and this is the upper-bound value of $K(f)$ for vibration at all frequencies above the second natural frrequency. Between the first and second natural frequencies the maximum value of $K(f)$ is 2·65, an increase of only 15 per cent above the upper bound of 2·3 observed at higher frequencies. These results support the use of correlations between the spatial maxima of dynamic stress and velocity at both resonant and non-resonant frequencies, and the use of resonant correlation ratios for generally conservative predictions at non-resonant frequencies. Predictions of

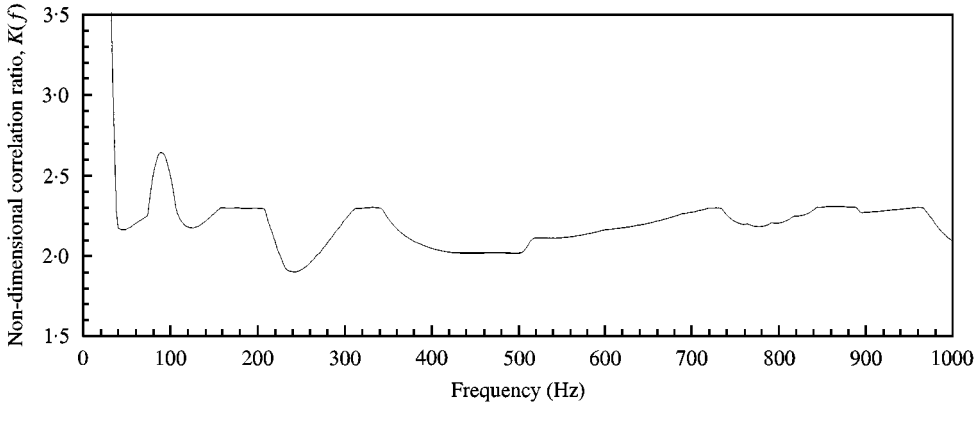

Figure 6. Calculated correlation ratio expressed as $K(f)$ for a point-excited clamped beam.

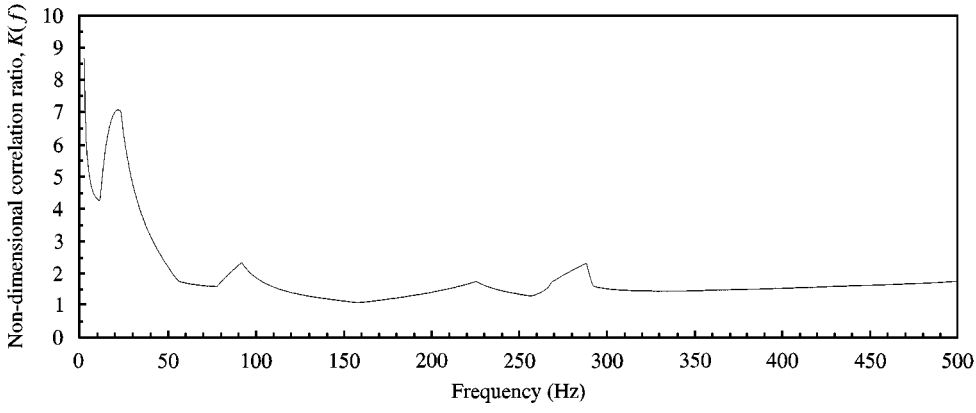

Figure 7. Calculated correlation ratio expressed as $K(f)$ for a point-excited simply supported beam with a 3·5 kg concentrated mass at $x = 0{\cdot}45$ m.

dynamic stress at non-resonant frequencies above the first natural frequency calculated using resonant correlation ratios are conservative by at most 20 per cent for this system.

5.5.2. *Clamped beam vibration below the first natural frequency*

For vibration at frequencies below the first natural frequency, $K(f)$ becomes infinitely large as frequency is decreased to zero since velocity tends to zero and dynamic stress tends to a finite, non-zero value. Correlation ratios are therefore of limited practical use in the prediction of dynamic stress from velocity at frequencies below the first natural frequency.

5.5.3. *Systems with a concentrated mass*

$K(f)$ is plotted in Figure 7 for a 0·9 m long simply supported beam with a 3·5 kg concentrated mass at $x = 0{\cdot}45$ m. The value of $K(f)$ is large at low frequency but decreases to a small bounded value at higher frequencies. Therefore, the same correlations apply to a system with a concentrated mass except that a large value of $K(f)$ must be used at low frequencies. The reasons for an increased value of $K(f)$ at low frequency are described in section 4.2.

5.6. PROPERTIES OF THE CORRELATION RATIO BETWEEN DYNAMIC STRESS AND VELOCITY

The correlation ratio between the spatial maxima of dynamic stress and velocity has a number of useful properties that make it of practical interest for the prediction of maximum dynamic stress from velocity. The main properties of the correlation ratio are that (i) it is largely frequency independent, (ii) it lies in a small range, and (iii) it is largely independent of structural details such as boundary conditions, geometry and dimensions. Furthermore, the same relationships are applicable to vibration at both resonant and non-resonant frequencies. These properties of the correlation ratio arise primarily from the fundamental relationship between the

propagating wave components of dynamic stress and velocity in equation (5), and the limited effect of evanescent waves on the magnitudes of the spatial maxima of dynamic stress and velocity (section 4). The main limitations with use of correlations between the spatial maxima of dynamic stress and velocity are that they are not applicable to vibration below the first natural frequency of a system, and special attention must be given to the effects of concentrated masses at the lowest natural frequencies of a system.

Other features of using correlations between dynamic stress and velocity are that (i) correlation ratios for resonant vibration are easily calculated using a normal mode model; (ii) resonant correlation ratios may be used at non-resonant frequencies for generally conservative predictions of maximum dynamic stress; (iii) approximate values of the correlation ratio may be assumed in most cases without recourse to calculations; (iv) the vibrational velocity data required for predictions is easily measured; and (v) post-processing of the measured vibrational velocity data for the prediction of maximum mean-square or peak dynamic stress is straightforward and may be performed directly within modern digital signal analyzers without the need for complicated computer processing.

6. EXPERIMENTS

Broad-band measurements of dynamic strain and velocity taken from some point-excited beam systems with classical boundary conditions are used in this section to demonstrate (i) farfield correlations between dynamic strain and velocity; (ii) the effects of evanescent waves on farfield correlations in nearfield regions; (iii) narrow-band spatial distributions of dynamic strain and predicted dynamic strain; (iv) spectral predictions of maximum dynamic strain obtained using spatially distributed measurements of velocity; and (v) crest factors for dynamic strain and velocity. The structures considered are a clamped beam, a simply supported beam, and a simply supported beam with a point constraint.

6.1. EXPERIMENTAL ARRANGEMENTS

The experiments were performed using a 0·9 m long, 0·04 m wide and 0·005 m thick steel beam with 13 semi-conductor foil strain gauges bonded along one-half of the beam on one side only. Since the device that was used to clamp the beam was 0·04 m long, the length of the beam when clamped was reduced to 0·82 m. The locations of the strain gauges for the different beam arrangements are listed in Table 1, and the experimental beam arrangements are drawn in Figure 8. The experimental results presented in this section are mainly for the clamped beam system.

The beam systems were excited using a Bruel and Kjaer (B&K)-Type 4809 vibration exciter powered by a B&K-Type 2706 power amplifier. Strain-gauge measurements were performed with Kulite semi-conductor strain gauges, Type S/ACP-120-300, which are considerably more sensitive than standard foil gauges and do not need to be operated in a bridge arrangement. The strain gauges were

TABLE 1

Strain gauge labels and strain gauge positions for each of the beam arrangements

Gauge	Simply supported (m)	Clamped (m)
0	0·047	0·007
1	0·065	0·025
2	0·1	0·06
3	0·135	0·095
4	0·17	0·13
5	0·205	0·165
6	0·24	0·2
7	0·275	0·235
8	0·31	0·27
9	0·345	0·305
10	0·38	0·34
11	0·415	0·375
12	0·45	0·41

powered with a constant current of 20 mA and had a calibration factor of 2400 V per unit strain (using a fixed gain of 10). Light-weight B&K-Type 4375 charge accelerometers were used with a B&K-Type 2636 charge amplifier for vibrational velocity measurements and either another accelerometer or a B&K-Type 8001 impedance head (positioned between the structure and the exciter) was used as the reference when measuring spatial distributions. Vibration data were collected using a Dual-Channel B&K-Type 2133 real-time frequency analyzer. This analyzer was used to obtain both one-twelth octave spectral measurements and digitized time-history measurements. The measured data were subsequently transferred to a personal computer (PC) for post-processing. The calibration of the velocity measurement system was tested using a B&K-Type 4291 calibrator.

6.2. NARROW-BAND SPATIAL DISTRIBUTIONS

Narrow-band spatial distributions of measured dynamic strain and predicted dynamic strain (predicted from measured velocity) for the first half of the clamped beam in Figure 8(b) are plotted in Figure 9 for the first and fourth resonant frequencies. The beam was excited by a point force at $x = 0{\cdot}635$ m using a white noise excitation signal. The experimental results in Figure 9 agree with the theoretical spatial distributions presented in section 4.1. These results show that (i) dynamic strain and velocity are simply related in the farfield away from the clamped boundaries; (ii) dynamic strain and velocity are not correlated in the nearfield region associated with a clamped boundary; (iii) farfield conditions do not occur at the lowest resonant frequency: (iv) the first velocity minimum away from a clamped boundary provides a useful demarcation between the nearfield and the farfield; and (v) that the spatial maxima of dynamic strain and velocity are increased

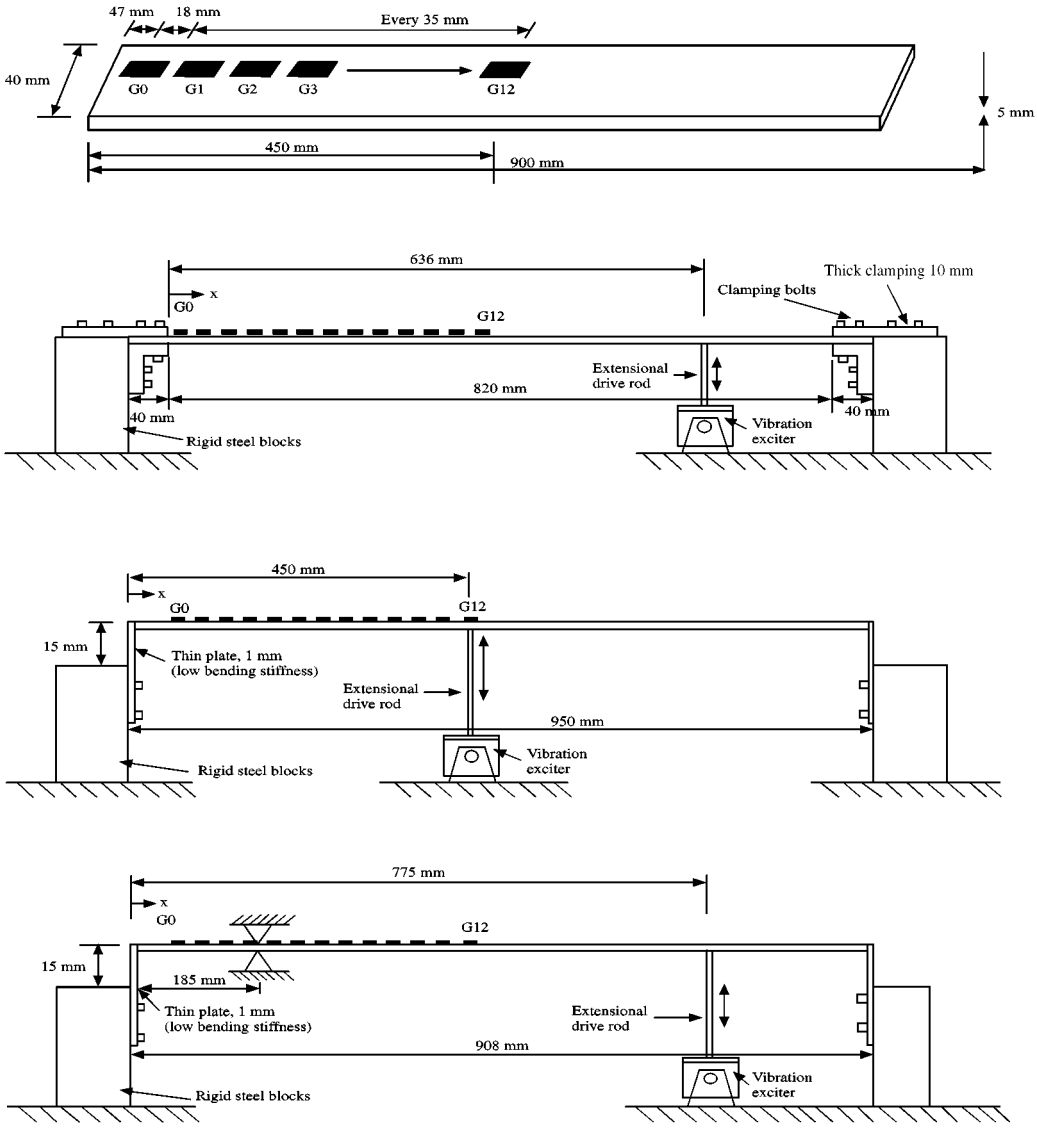

Figure 8. Experimental beam arrangements. (a) Strain-gauged beam. (b) Clamped beam. (c) Simply supported beam. (d) Simply supported beam with a point constraint.

above maixmum farfield levels due to evanescent wave effects, but by different amounts and at different locations. Maximum dynamic strain occurs at the clamped boundary and the increase in dynamic strain at this location in comparison with maximum farfield levels is referred to as dynamic strain concentration.

Spatial distributions at a resonant and a non-resonant frequency of the simply supported beam in Figure 8(c) are plotted in Figure 10. At resonance there are no evanescent waves associated with either the pinned boundaries or the point of excitation and the measurements of dynamic strain and velocity are related by the

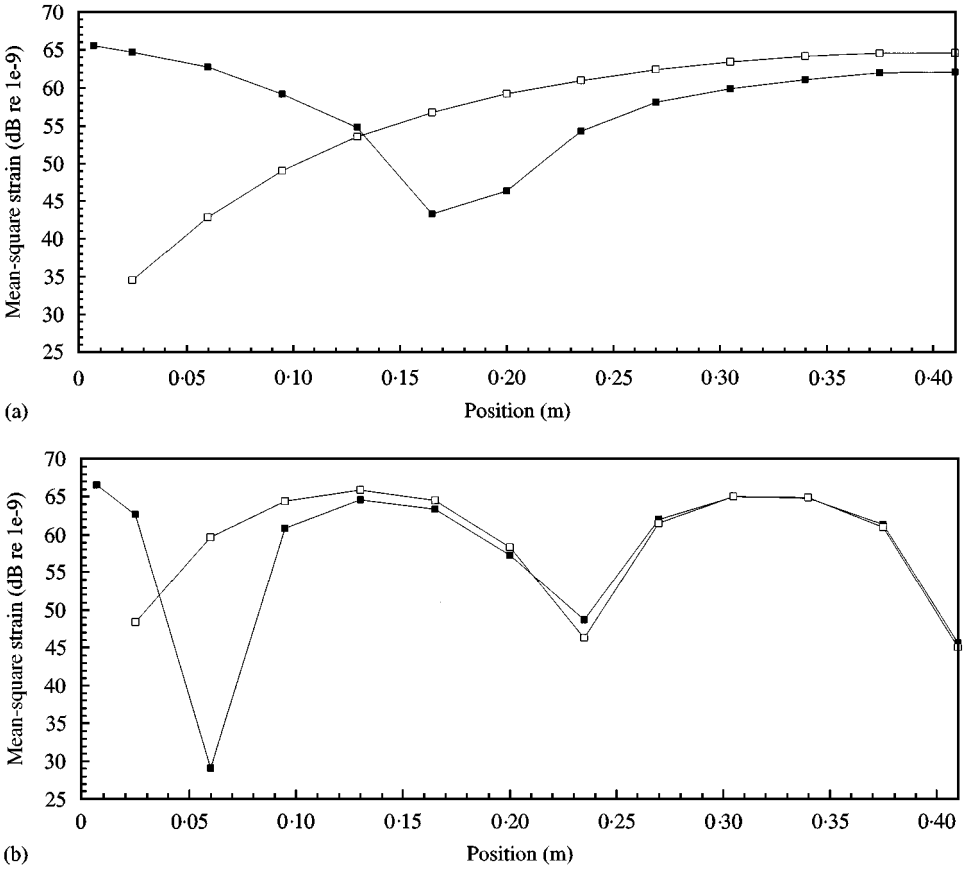

Figure 9. Measured and predicted dynamic strain spatial distributions of the clamped beam excited at $x = 0{\cdot}635$ m by white noise (1/12-octave bands). (—■— measured; —□— predicted). (a) 1st resonant frequency (39 Hz). (b) 4th resonant frequency (325 Hz).

farfield correlation ratio at all positions along the beam. However, at the slightly higher non-resonant frequency in Figure 10(b), there are evanescent waves emanating from the point of excitation which affect the correlation of dynamic strain and velocity in the region of the point force applied at $x = 0{\cdot}45$ m.

6.3. FARFIELD PREDICTIONS

Frequency-domain and time-domain predictions of dynamic strain based on the use of farfield relationships from section 2.3 are presented in Figure 11 for the position $x = 0{\cdot}34$ m of the clamped beam system in Figure 8(b). The selected position lies in the farfield at all frequencies above the second resonant frequency of the clamped beam. The beam was excited with white noise using a point force applied at $x = 0{\cdot}635$ m. There is very good agreement between the measured and predicted dynamic strain autospectra at frequencies above the second resonant

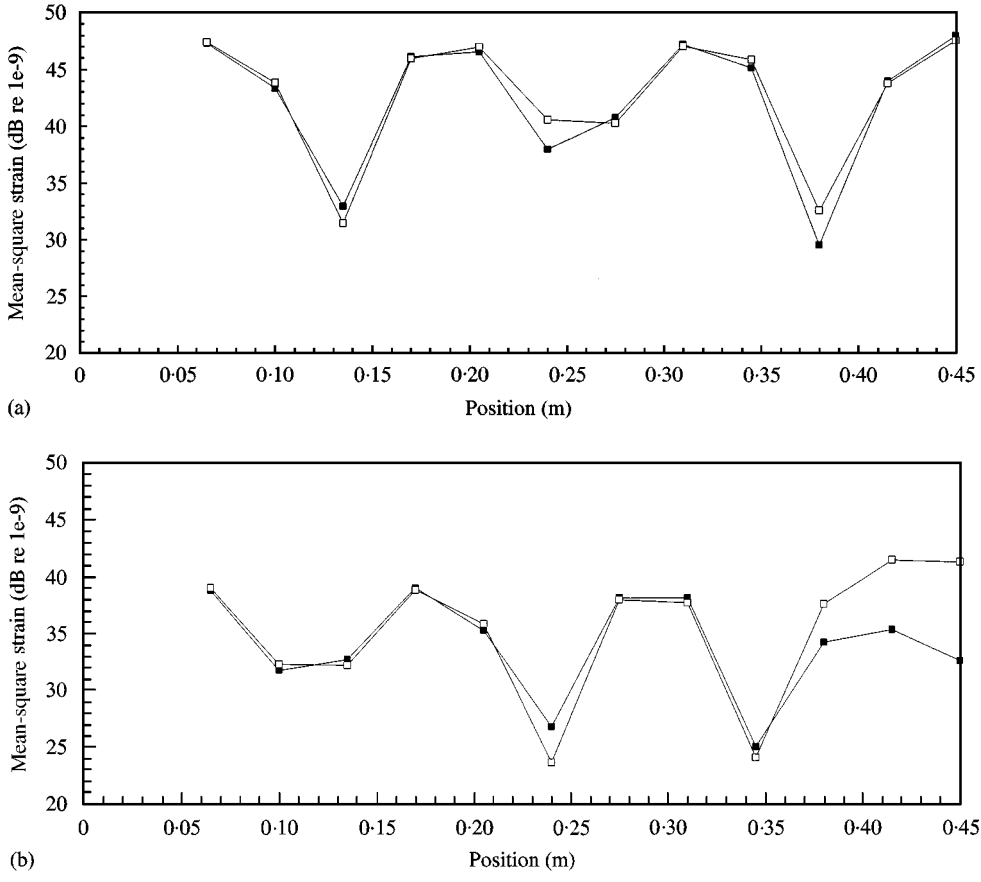

Figure 10. Measured and predicted dynamic strain spatial distributions of simply supported beam excited at $x = 0{\cdot}45$ m by white noise (1/12-octave bands). (—■— measured; □— predicted). (a) 4th resonant frequency (688 Hz). (b) Non-resonant frequency between the 4th and 5th resonant frequencies (818 Hz).

frequency. At the second resonant frequency and below, the measured dynamic strain is overpredicted due to evanescent wave effects. There is also good agreement between the measured and predicted dynamic strain time histories except for some overprediction of dynamic strain level due to low-frequency evanescent wave effects.

Processing procedures: The frequency-domain predictions of dynamic strain were obtained by scaling the measured velocity autospectrum by the farfield correlation ratio for dynamic strain according to equation (8). The predicted dynamic strain time histories were obtained from measured velocity time histories by performing a phase shift of 90° in the frequency-domain (by using Fourier transforms and convolution) and scaling the velocity time history by the farfield correlation ratio for dynamic strain [see equation (10)]. A phase shift was necessary to account for the phase shift between the propagating wave components of dynamic strain and velocity.

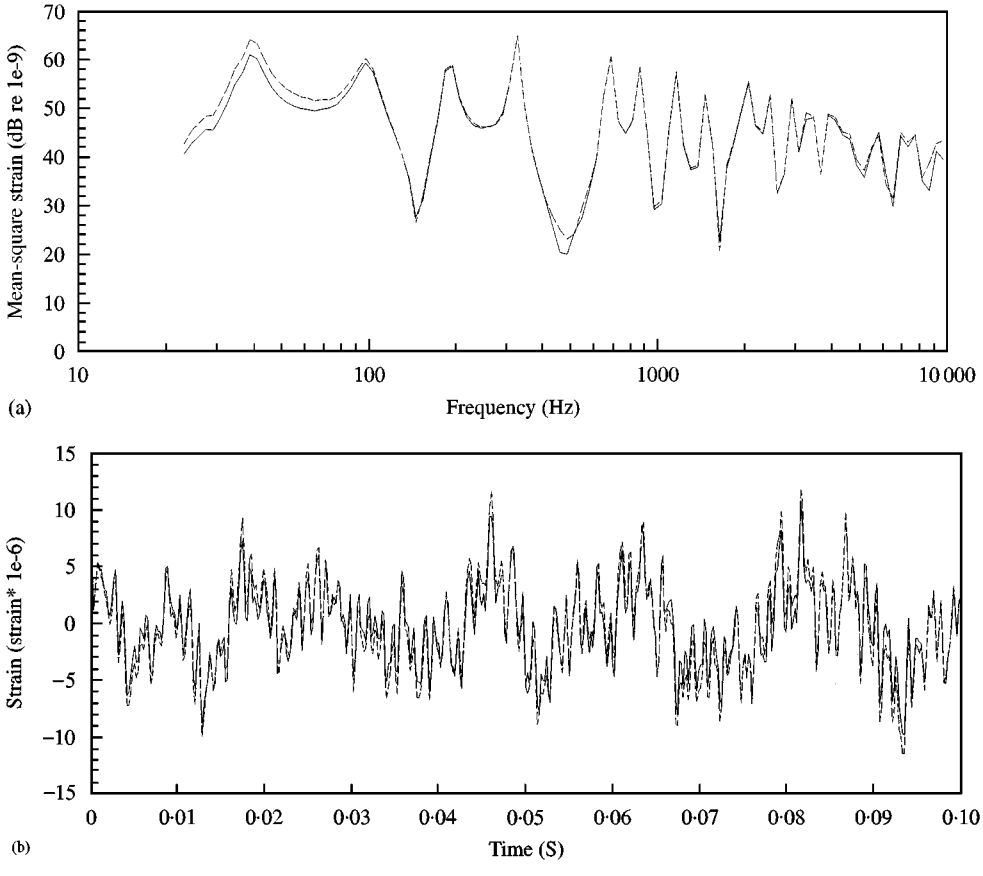

Figure 11. Measured and predicted dynamic strain at $x = 0{\cdot}34$ m of the clamped beam excited by white noise. (—— Measured; - - - - predicted). (a) Frequency-domain prediction. (b) Time-domain prediction.

6.4. NEARFIELD PREDICTIONS

Frequency-domain and time-domain predictions of dynamic strain are presented in Figure 12 for a location which lies in the nearfield of the clamped beam system in Figure 8(b) at frequencies up to 1 kHz. In Figure 12(a), dynamic strain is observed to be underpredicted at frequencies below 200 Hz, overpredicted at frequencies between 200 Hz and 1 kHz, and accurately predicted at frequencies above 1 kHz. Since the uncorrelated low-frequency components are significant to the beam response, they have a significant adverse effect on the time–domain correlation of dynamic strain and velocity at all points in time.

The frequency-domain predictions vary from under-predicting to over-predicting due to the opposite effects of evanescent waves on dynamic strain and velocity, and the changing location of the measurement position with frequency relative to the spatial distributions of dynamic strain and velocity (due to decreasing wavelength). As a result of evanescent wave effects on dynamic strain and velocity, dynamic strain cannot be predicted from the velocity measured at the same location if nearfield conditions exist.

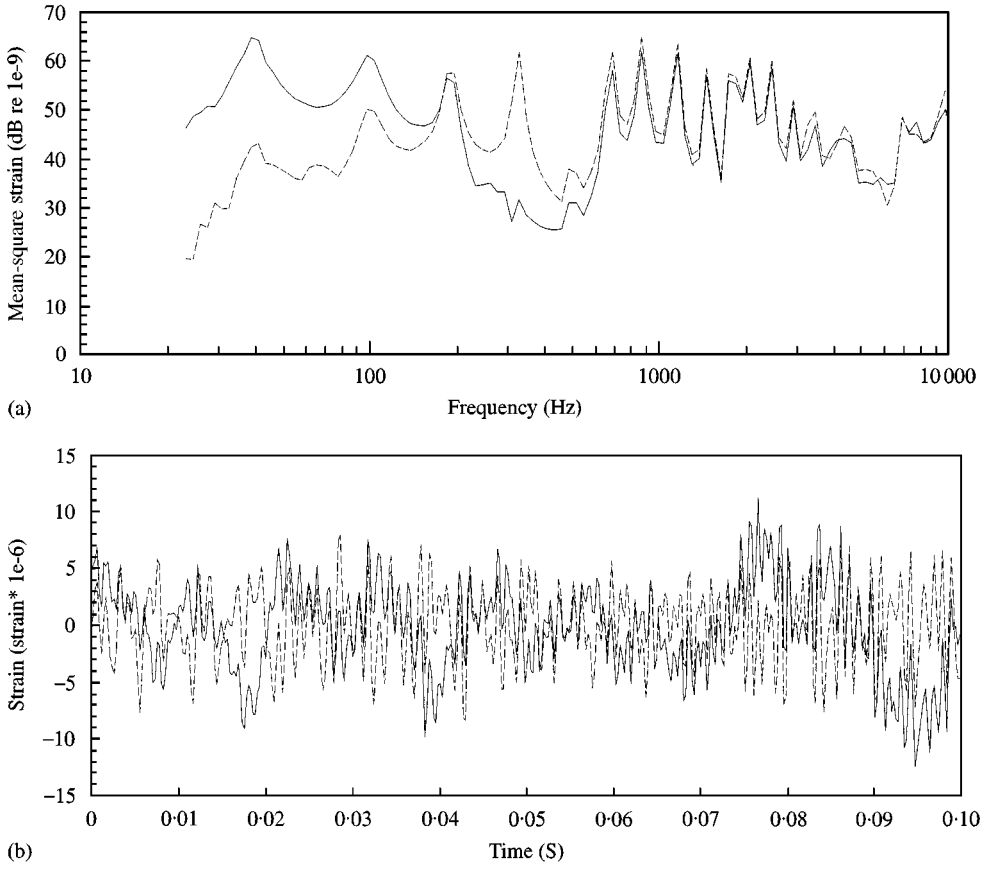

Figure 12. Measured and predicted dynamic strain at $x = 0{\cdot}06$ m of the clamped beam excited by white noise. (—— Measured; - - - - predicted). (a) Frequency-domain prediction. (b) Time-domain prediction.

6.5. SPECTRAL PREDICTIONS OF MAXIMUM DYNAMIC STRAIN

In order to predict maximum overall dynamic strain in broad-band excited systems, it was proposed in section 5 that correlations between the spatial maxima of dynamic strain and velocity be used in place of relationships between dynamic strain and velocity at the same location. This was necessitated by evanescent wave effects which prevent the correlation of dynamic strain and velocity at a point in the nearfield. The procedure is to construct a spectrum of the spatial maximum velocity in each frequency band for the whole beam and scale this spectrum by the farfield correlation ratio for dynamic strain. A factor is then added to take into account evanescent wave effects.

6.5.1. *Clamped beam system*

The autospectrum of predicted maximum dynamic strain for the clamped beam system is compared in Figure 13 with the measured autospectrum at the position of maximum overall dynamic strain. A factor of 1 dB was used to take into account

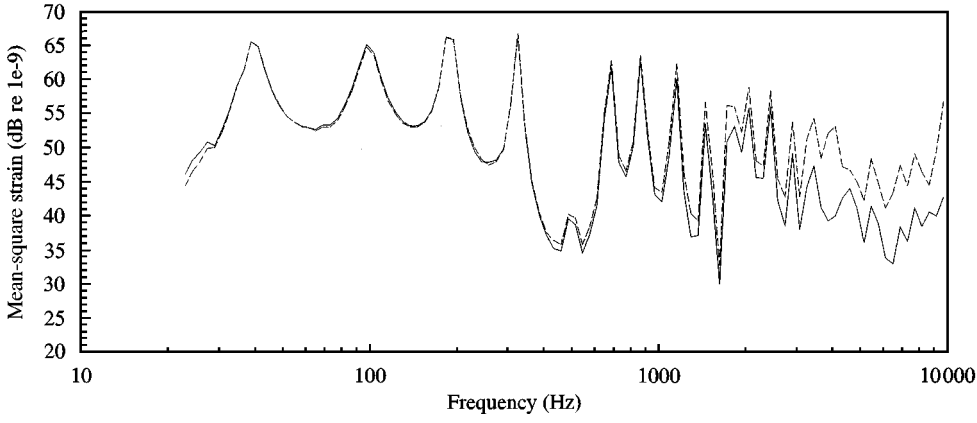

Figure 13. Measured and predicted dynamic strain of a clamped beam excited by white noise. Predicted using the sqatial maximum velocity in each frequency band, the farfield correlation ratio and a correction factor of 1 dB. (—— Measured; - - - - predicted).

evanescent wave effects. The predicted spectrum accurately predicts the measured dynamic strain at frequencies up to 1 kHz and overpredicts at frequencies above 1 kHz Dynamic strain is overpredicted at high frequencies since the strain gauge was not located close enough to the clamped boundary for measurement of the maximum dynamic strain associated with short-wavelength, high-frequency components. These high-frequency errors demonstrate a general difficulty with measuring maximum dynamic strain at high frequencies with finite-length strain gauges.

6.5.2. *Simply supported beam system*

The same procedure was also applied to the prediction of maximum dynamic strain in a broad-band excited simply supported beam, except that no factor was added for evanescent wave effects since there is no dynamic strain concentration for vibration of this system at resonance. The measured and predicted dynamic strain autospectra are plotted in Figure 14. At resonance there is good agreement between the measured and predicted dynamic strain autospectra, but at non-resonant frequencies the predicted dynamic strain varies between under-predicting and over-predicting due to nearfield effects associated with the exciting force.

6.5.3. *Simply supported beam with a point constraint*

Predictions of overall dynamic strain are presented in Table 2 for a simply supported beam excited by white noise with a point constraint at $x = 0{\cdot}185$ m. Since this system consists of two sub-systems, it can be analyzed as either a single system or two sub-systems. Results for the predicted dynamic strain using both approaches are presented in Table 2. These predictions are compared with (i) the maximum measured overall dynamic strain and (ii) the maximum measured overall dynamic strain calculated from an autospectrum constructed of the measured spatial maximum dynamic strain in each frequency band. Autospectral predictions

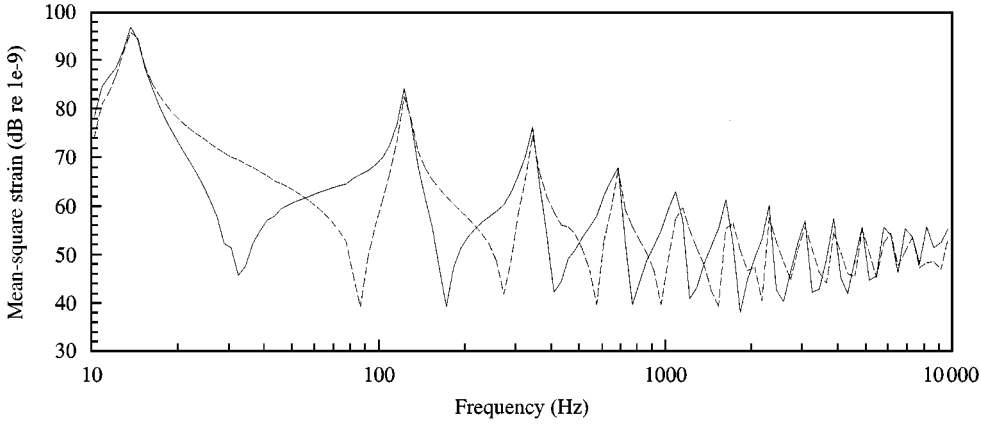

Figure 14. Measured and predicted dynamic strain at the location of maximum overall strain for a simply supported beam excited by white noise. (—— measured at $x = 0{\cdot}45$ m; - - - - predicted maximum dynamic strain in each frequency band).

TABLE 2

Measured and predicted overall dynamic strain

	Short sub-system (dB)	Long sub-system (dB)	Whole beam (dB)
Measured	62·6	65·0	65·0
Measured, spatial maximum each frequency	64·1	66·5	66·9
Predicted, spatial maximum each frequency	61·8	66·9	67·4

using the single-system approach are presented in Figures 15 and 16 for the sub-system approach (short section only).

Predictions based on the analysis of the beam as a single system provide conservative predictions, whereas the use of a sub-system approach in the case of the short sub-system leads to non-conservative predictions. The sub-system approach is non-conservative due to a retarded velocity response at low frequencies (Figure 16). Therefore, the sub-system approach should not be used if low-frequency components are significant. At high frequencies either approach may be used.

6.6. CREST FACTORS FOR THE PREDICTION OF MAXIMUM PEAK DYNAMIC STRAIN

Due to the nearfield effects discussed previously, spectral methods must be used for the prediction of maximum overall dynamic strain when using strain-velocity correlation. The use of a crest factor permits these predictions of maximum overall

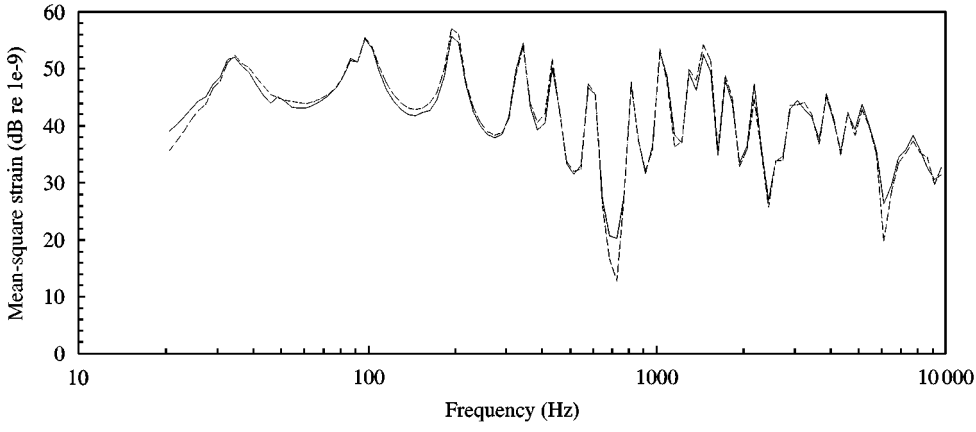

Figure 15. Measured and predicted dynamic strain spatial maxima in each frequency band of the simply supported beam constrained at $x = 0{\cdot}185$ m and excited at $x = 0{\cdot}775$ m by white noise. (— measured; – – – predicted).

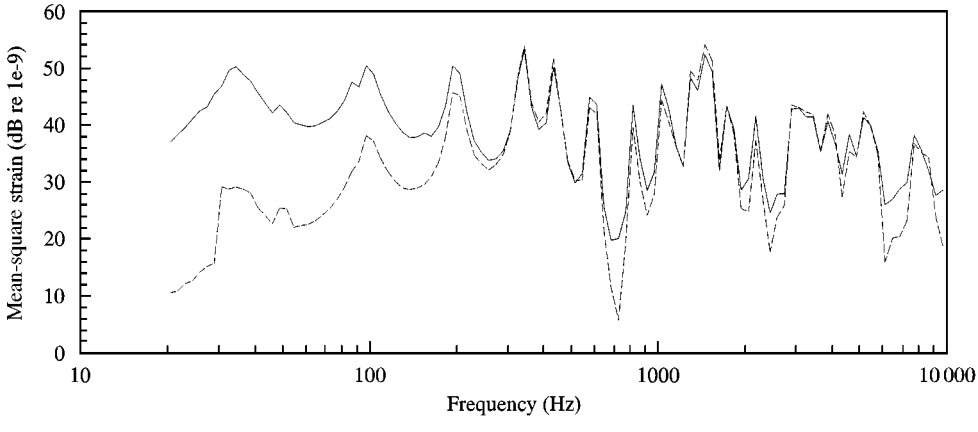

Figure 16. Measured and predicted dynamic strain spatial maxima in each frequency band for the short section of the simply supported beam constrained at $x = 0{\cdot}185$ m and excited at $x = 0{\cdot}775$ m by white noise. (— measured; – – – predicted).

dynamic strain to be used for the prediction of the maximum peak dynamic strain in the time-domain (see section 5.3.3). Crest factors are given in Table 3 for excitation of the clamped beam system in Figure 8(b) by white noise. These crest factors were calculated from measurements of (i) dynamic strain and velocity at the same position in the farfield; (ii) dynamic strain in the nearfield and velocity in the farfield; and (iii) the excitation force signal. The ratio of the peak value to the root-mean-square value ranges from 4·0 to 4·5, and is similar for dynamic strain, velocity and excitation force.

7. SUMMARY AND CONCLUSIONS

The spatial distributions of dynamic strain and velocity in randomly excited beams have been reported on in this paper. Relationships between dynamic strain

TABLE 3

Crest factors for whie-noise excitation of a clamped beam

Measurement	r.m.s.	Peak	Ratio of peak to r.m.s.	Ratio of peak to ($\sqrt{2}$* r.m.s.)
Strain $x = 0{\cdot}34$ m	3·9 μ	17·7 μ	4·5	3·2
Velocity, $x = 0{\cdot}34$ m	13·2 mm/s	55·1 mm/s	4·2	2·9
Strain, $x = 0{\cdot}007$ m	7·2 μ	27·0 μ	4·3	3·0
Velocity, $x = 0{\cdot}34$ m	13·2 mm/s	55·1 mm/s	4·2	2·9
Excitation force	6·16 N	24·7 N	4·0	2·8
Strain, $x = 0{\cdot}007$ m	7·2 μ	27·1 μ	4·3	3·0

and velocity were also investigated. The specific results of this work are summarized as follows:

1. Hunt [1] and Ungar [2] have shown that the propagating wave components of dynamic bending strain and velocity at the same spatial position are related by $\xi_{FF}/v_{FF} = y_m k_B^2/\omega$ for the transverse vibration of beams. The ratio of dynamic bending strain to velocity in farfield regions is defined as the farfield correlation ratio. The farfield correlation ratio for flexural vibration of a beam is frequency independent and is a function of only the non-dimensional shape factor.
2. Simple farfield relationships between dynamic strain and velocity at the same spatial position cannot be used to predict dynamic strain from velocity in the nearfield regions of beams, due to the opposite effects of evanescent waves on the propagating wave components of dynamic strain and velocity. These opposite effects result from the opposite phase of evanescent waves in the travelling wave solutions for dynamic strain and velocity.
3. Evanescent waves increase the spatial maximum levels of dynamic strain and velocity above the spatial maximum levels of the propagating wave components of the response. Due to evanescent wave effects, the propagating wave components of dynamic strain and velocity are increased by different amounts and at different locations.
4. In the case of low-frequency non-resonant vibration below the first resonant frequency of a structure, or low-frequency resonant vibration of a structure with a concentrated mass, evanescent waves increase dynamic strain but decrease velocity in comparison with the propagating wave components of the response.
5. Increased dynamic strain due to evanescent wave effects is defined as dynamic strain concentration. Dynamic strain concentration occurs in boundary regions and near discontinuities. Dynamic strain concentration is different to, and considered to be independent of, additional geometric stress concenration effects.
6. The spatial extent of dynamic strain concentration decreases as the wavenumber of evanescent waves increases. This results in short regions of high dynamic strain which are difficult to measure using strain gauges.

7. Relationships for the prediction of dynamic strain from velocity are based on the correlation of dynamic strain and velocity spatial maxima in narrow frequency bands. Formal relationships are defined by using the spatial maxima of the propagating wave components of the response in the farfield relationship between dynamic strain and velocity, and by incorporating factors for the effects of evanescent waves on the spatial maxima of the propagating wave components of dynamic strain and velocity.
8. The use of spatial maxima for dynamic strain and velocity in narrow frequency bands for the prediction of dynamic strain takes into account (i) the different locations of maximum dynamic strain and maximum velocity due to evanescent wave effects; and (ii) variations in the positions of maximum dynamic strain and maximum velocity with frequency.
9. The ratio of maximum dynamic bending strain to maximum velocity is defined as the correlation ratio. The correlation ratio can be defined theoretically or experimentally. The correlation ratio is based with a spatially distributed set of narrow-band velocity measurements to obtain conservative predictions of spatial maximum dynamic bending strain in randomly vibrating structures.
10. The correlation of dynamic strain and velocity spatial maxima applies at both constant and non-resonant frequencies, since farfield relationships between dynamic strain and velocity are independent of resonance, and the effects of evanescent waves are both bounded and lie in a small range.
11. The correlation of dynamic strain and velocity spatial maxima applies to both narrow-band and broad-band excited structures, since the relationships and procedures for the prediction of dynamic strain from velocity using strain–velocity correlation are applicable to vibration at any frequency and over any frequency range (at or above the first resonant frequency).

The experimental data presented in this paper demonstrate relationships between dynamic strain and velocity and the effects of evanescent waves on the propagating wave components of dynamic strain and velocity. The results of the experimental work support the theoretical results presented. The most important conclusions of this paper are that (i) there exists largely frequency-independent correlations between dynamic strain and velocity which have a firm theoretical basis; (ii) spatial maximum levels of dynamic strain can be predicted from simple measurements of vibrational velocity; (iii) the relationships apply equally to narrow-band and broad-band vibration; (iv) numerical methods such as the finite-element method can be used to calculate the correlation ratio between dynamic stress and velocity for the prediction of maximum dynamic stress or strain.

REFERENCES

1. F. V. Hunt 1960 *The Journal of the Acoustical Society of America* **32**, 1123–1128. Stress and strain limits on the attainable velocity mechanical vibration.
2. E. E. Ungar 1962 *Journal of Engineering for Industry* **84**, 149–155. Maximum stresses in beams and plates vibrating at resonance.
3. J. C. Wachel *et al.* 1985 *EDI Report 85-305. Engineering dynamics Incorporated, San Antonio Texas.* Vibrations in reciprocating machinary and piping systems.

4. S. M. Stearn 1970 *Ph.D. Thesis.* Stress distributions in randomly excited strucures.
5. R. H. Lyon 1975 *Statistical Engergy Analysis of Dynamical systems: Theory and Applications.* Cambridge: the MIT Press.
6. M. P. Norton and F. J. Fahy 1988 *Noise Control Engineering Journal* **30**, 107–117. Experiments on the correlation of dynamic stress and strain with pipe wall vibrations for statistical energy analysis applications.
7. S. M. Stearn 1971 *Journal of Sound and Vibration* **15**, 353–365. The concentration of dynamic stress in a plate at a sharp change of section.
8. E. E. Ungar 1961 *The Journal of the Acoustical Society of America* **33**, 633–639. Transmission of plate flexural waves through reinforcing beams: dynamic stress concentrations.
9. D. G. Karczub 1996 *Ph.D. Thesis*, *The University of Western Australia.* The prediction of dynamic stress and strain in randomly vibrating structures using vibrational velocity measurements.